Solid Phase Synthesis of *N*-Alkyl-bis-*o*-aminobenzamides for Metal Ion Sensing Based on a Fluorescent Dansyl Platform

G. Pina-Luis, A. Ochoa-Terán, and I. A. Rivero*

Graduate Center and Research of Technological Institute of Tijuana, Apartado Postal 1166. 22000. Tijuana, B.C. México

Received May 7, 2008

In this paper, we report the synthesis on Merrifield's resin of alkyl-bis-*o*-aminobenzamides labeled with a fluorescent dansyl group for use in metal ion recognition. The influence of alkyl groups with different long chains ($n = 1, 2, 4, 6$) on the spectral fluorescence characteristics was studied. The sensing properties of the beads were evaluated by packing the resins into a flow-through cell for use in a FIA (flow injection analysis) format. Results demonstrated that for those materials with a longer alkyl chain, the fluorescence emission increased upon Li^+, Na^+, K^+, Ca^{2+}, and Mg^{2+} addition with a higher sensitivity for Mg^{2+}. On the contrary, a fluorescence quenching was observed when Cu^{2+}, Fe^{3+}, or Zn^{2+} ions were added. The potential applicability of the sensing approach described in this paper for magnesium ions and the sensing response mechanism are outlined.

Introduction

There is significant interest in the design and synthesis of fluorescent sensors for detection of metal ions in many scientific fields, such as biology, clinical biochemistry, and environmental science. The design of abiotic receptors to achieve the recognition process with a simultaneous transduction of a human-observable change of signal (absorbance, fluorescence, phosphorescence, etc.) has been developed significantly over the past 30 years.[1] Among the different analytical transduction methodologies available for detection of metal ions, fluorescence offer several advantages. Fluorescence is a multidimensional technique, and metal ion recognition can be observed via changes in emission intensity, quantum yield, wavelength, lifetime, and chirality.[2,3] Also, fluorescence affords a nondestructive way of obtaining real-time, online information with high sensitivity and selectivity. Therefore, considerable efforts have been made to develop selective and sensitive fluorescent sensors for metal ions. In fact, we are involved in the development of abiotic receptors designed on the basis of the photoinduced electron transfer (PET) process.[4−7] A simplified picture of this process is the donor−acceptor (D−L−A) system (Scheme 1). The donor group is covalently bound, through a rigid or flexible linker unit, to the acceptor. Upon photoexcitation to an excited state, electron transfer leads to charge-separated species. An important issue for the successful use of these supramolecular systems is stabilization of the charge-separated species to prevent the back electron transfer. Several factors control the electron transfer process: the oxidation potential of the donor, the reduction potential of the acceptor,[8] orientation, and distance between donor and acceptor and the nature and length of the linker unit.[9,10]

Immobilization of fluorescent chemosensors on solid supports for developing optical sensors should result in improved analytical performance characteristics, such as continuous readout, lower reagent consumption, and the possibility of using the sensor in solvents, where the free molecule displays low solubility. In particular the immobilization of the PET probe on a solid support is a much more difficult task as the sensing properties can be drastically changed upon immobilization.[11,12] De Silva et al.[13] reported that the immobilized binding site local concentration dictates the response and the ultimate analytical performance of the system. Studies and applications of fluorescent sensor immobilized on solid phase have been successfully performed in batch[14−18] and using a flow-through optosensing approach.[19] We have reported fluorescent chemosensors on solid support in a flow-through approach, for metal ions,[20,6] and for fructose recognition.[5]

A major objective in our research has been the design and synthesis of D−L−A systems bound to solid supports for metal ion sensing using the fluorescence off/on switching based on a PET mechanism in a flow-through approach. In this paper, attention is focused on the design of D−L−A systems to examine three aspects: (a) the efficiency of the electron transfer process as a function of metal ion binding, (b) the effect of chain length on the sensing process, and (c) the analytical potential of the D−L−A systems. The model systems studied include *o*-aminobenzamide-brigde-*o*-aminobenzamide and *o*-aminobenzamide-brigde-*o*-aminobenzamide-dansyl dyads **2** and **3** (see Scheme 2).

In Scheme 3 the relationship between D−L−A structure and orbital energy levels is shown, along with the off/on switching mechanism for sensing. Binding of a metal ion

* E-mail: irivero@tectijuana.mx. Phone: (664) 6233772. Fax: (664) 6234043.

10.1021/cc8000772 CCC: $40.75
Published on Web 12/11/2008

Scheme 1. Photoinduced Electron Transfer Process (PET)

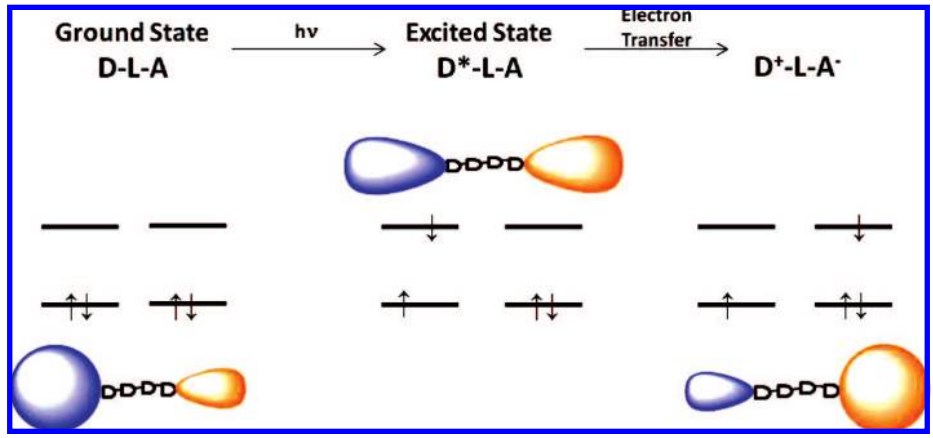

Scheme 2. Synthesis of Alkyl-bis-*o*-aminobenzamide Dansyl Resins

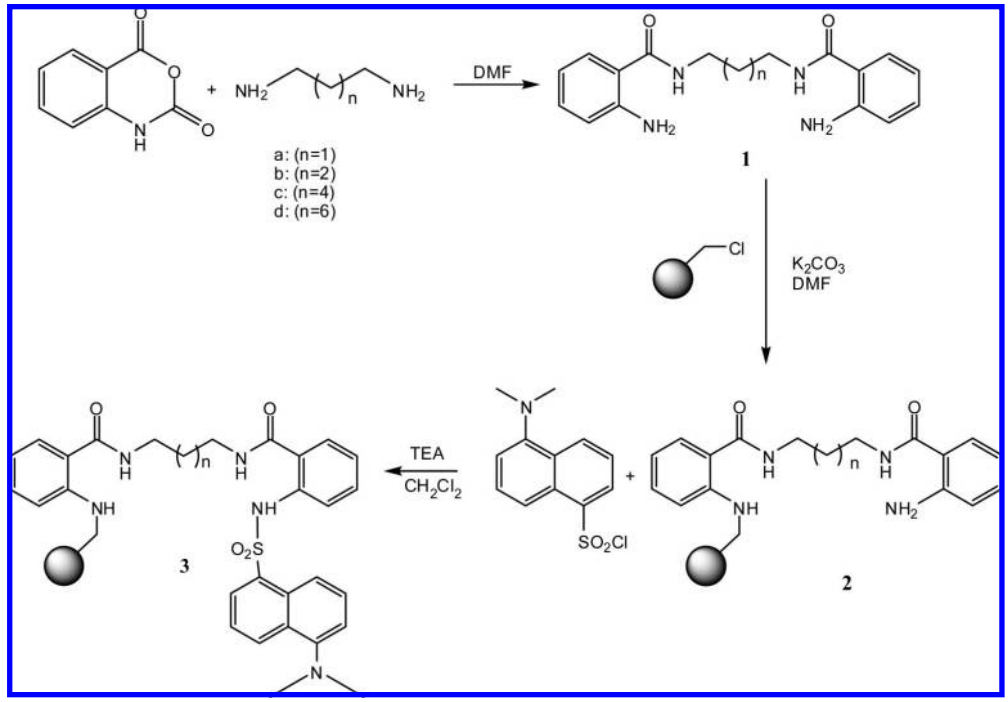

will change the redox potential of the donor so that the relevant HOMO becomes lower in energy than that of the fluorophore; consequently, PET is no longer possible and fluorescence quenching is suppressed.

Results and Discussion

***N*-Alkyl-bis-*o*-aminobenzamide Dansyl Immobilization.** Merrifield resin, extensively used in the solid phase synthesis of many molecules,[21−23] was used for preparation of immobilized *N*-alkyl-bis-*o*-aminobenzamide dansyl fluorescent recognition units. The synthesis of immobilized *N*-alkyl-bis-*o*-aminobenzamide dansyl into resin beads was readily achieved by the syntheses route outline in Scheme 2. Our synthetic route involves the initial reaction of 2 equiv of isatoic anhydride with 1 equiv of the corresponding alkyldiamine reagent in dimethylformamide to obtain alkyl-bis-*o*-aminobenzamides **1**(**a**−**d**). The alkyl-bis-*o*-aminobenzamides obtained were coupled to the Merrifield resin through a nucleophilic displacement of chloride group catalyzed by K_2CO_3 and using dimethylformamide (DMF) as solvent to yield the alkyl-bis-*o*-aminobenzamide resins **2**(**a**−**d**), with 80−88% conversions determinate under the volumetric Volhard analysis method.[24] Although the *N*-alkyl-bis-*o*-aminobenzamide **1** is bifunctional compound, the cross-coupling reaction with the solid support is less favorable than a single coupling. This is due to the long distance between each linker on the solid support, which is approximately 100 Å, calculated considering the load per gram of resin and its volume. Finally, the reaction of dansyl chloride with resins **2**(**a**−**d**), triethylamine as a base, and dichloromethane as a solvent gave the desired alkyl-bis-*o*-aminobenzamide dansyl resins **3**(**a**−**d**). These materials were washed with dichloromethane and methanol and dried under high vacuum for 12 h. These products were synthesized with high conversion (80−90%). The immobilized **1**(**a**−**d**) were cleaved from the polymer by treatment with a solution of trifluoroacetic acid-dichloromethane (1:10) for 30 min under ultrasonic conditions. The resins were filtered and 1 μL of the washing solution was directly injected on an ESI-MS for analysis. The corresponding molecular ions $[M + H]^+$ were obtained

Scheme 3. Off/On Switching Mechanism for Sensing

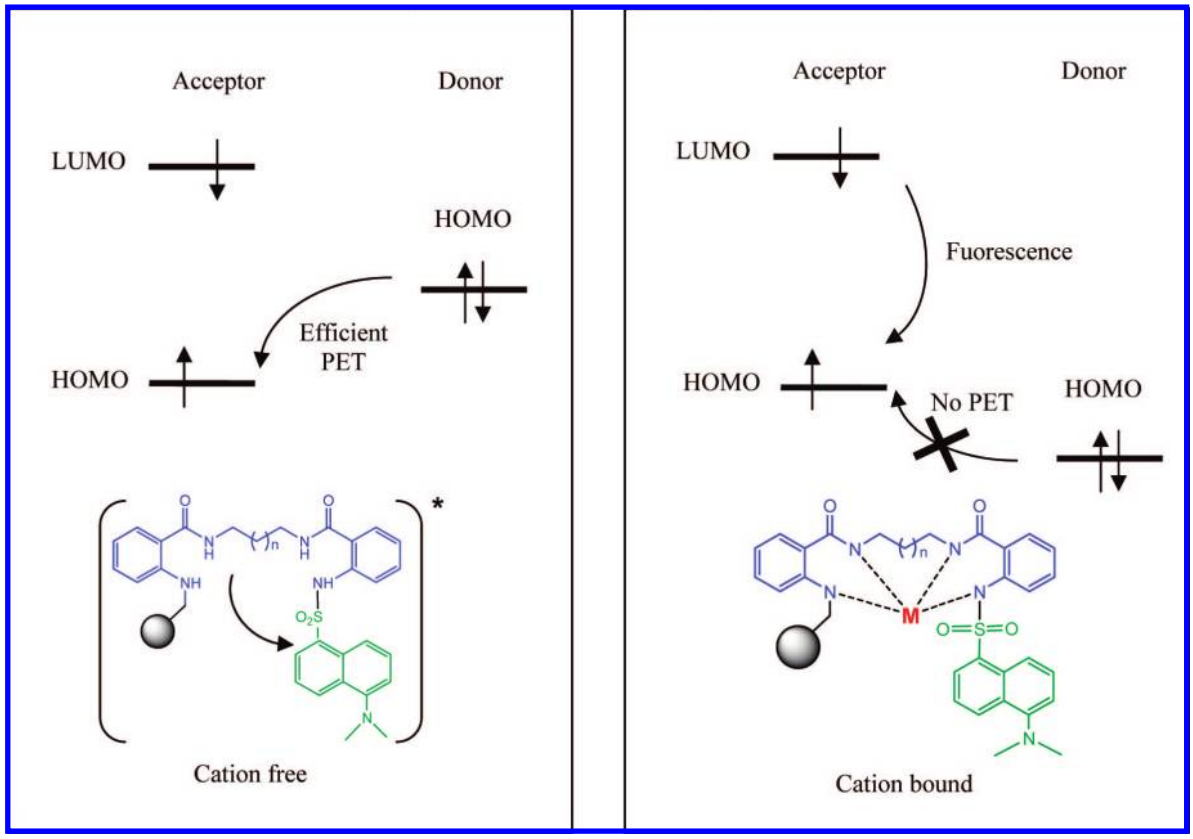

confirming the presence of the *N*-alkyl-bis-*o*-aminobenzamide group on the polymer support.

Mass Spectra Analysis. A simple method for the analysis of polymer-supported species based on mass spectrometry direct-insertion and electronic impact ionization was developed by our group.[25] Thermal cleavage on the benzylic position of the resins is promoted operating the instrument at high temperature and high vacuum conditions. Polymer degradation does not interfere in the determination of the molecular weight of compounds attached to the resin. Polymer-supported compounds were characterized by MS while still bound to the resins, avoiding time-consuming cleavages. Molecular weight and fragmentation pattern of all the supported molecules were exactly determined.

Fluorescence Characteristics. The fluorescence spectra of **1**, **2**, and **3**(**a**−**d**) derivatives (Scheme 2) were performed in order to evaluate how the structural changes at the different synthesis stages influence the spectral characteristics of the materials. The excitation and emission fluorescence spectra of the raw Merrifield resin, **2a** and **3a**, derivatives are shown in Figure 1.

As can be seen, the Merrifield resin showed low fluorescence intensity compared to the **2a** and **3a** derivatives. Attaching the propyl-bis-*o*-aminobenzamide (BOAB) deriva-

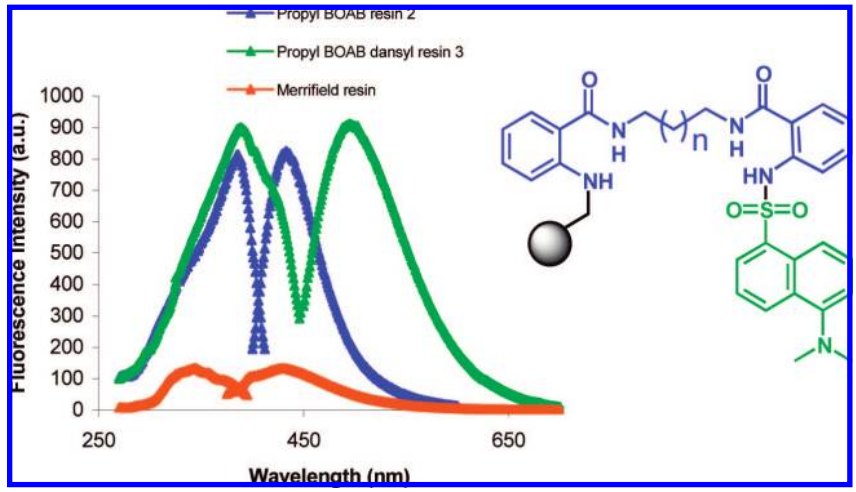

Figure 1. Excitation and emission spectra of dry resin beads for (a) Merrifield resin (λ_{exc} = 348 nm, λ_{em} = 436 nm), (b) propyl-bis-*o*-aminobenzamide bound to Merrifield resin (**2a**) (λ_{exc} = 377 nm, λ_{em}= 433 nm), (c) propyl-bis-*o*-aminobenzamide dansyl bound Merrifield resin (**3a**), (λ_{exc} = 390 nm, λ_{em} = 495 nm).

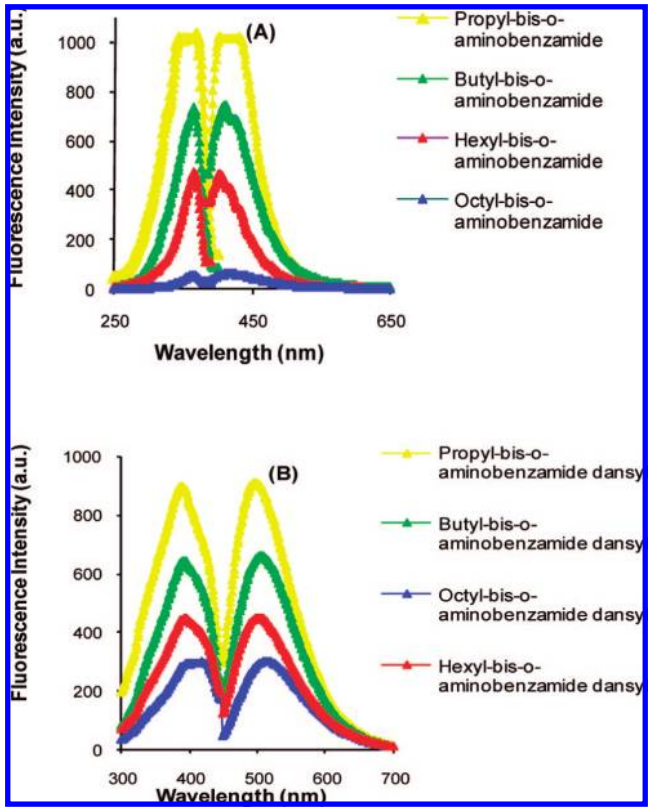

Figure 2. Fluorescence spectra of (A) *N*-alkyl-bis-*o*-aminobenzamide **2**(**a**−**d**) and (B) *N*-alkyl-bis-*o*-aminobenzamide dansyl **3**(**a**−**d**) bound to Merrifield resin.

tive is evidenced by a drastic increase in the fluorescence intensity along with a red-shift (ca. 30 nm) of the excitation maximum. The luminescence properties can be attributed to the ability of the chromophore to delocalize charge over both carbonyl−benzyl−amine groups in the molecular excited state. On the other hand, compared to the raw Merrifield resin, attachment of the BOAB dansyl derivative yielded ca. a 10-fold increase in fluorescence intensity and the emission maximum was red-shifted ca. 60 nm. The emission from **3a** observed at 495 nm may be associated to charge delocalization between the dansyl and the adjacent carbonyl−benzyl−amine group.

Fluorescence spectra of *N*-alkyl-bis-*o*-aminobenzamide **2**(**a**−**d**) and *N*-alkyl-bis-*o*-aminobenzamide dansyl **3**(**a**−**d**) bound to Merrifield resin is showed in Figure 2A and B, respectively. As observed, the excitation and emission spectra of **2**(**a**−**d**) series presented the same excitation and emission maximum wavelengths, regardless the alkyl chain length. However, fluorescence intensity increased as the length of the alkyl chain decreased.

A similar behavior was observed with the **3**(**a**−**d**) series. We could observe that there was a linear dependence of the fluorescence intensity on the decreasing length of the chain for both *N*-alkyl-*o*-aminobenzamide and *N*-alkyl-*o*-aminobenzamide dansyl derivatives (Figure 3). These facts may be explained in terms of a twisted conformation of the molecule as the length of the spacer chain increased, allowing only a partial conjugation in the molecule backbone. Also, as the length of the spacer increased the possibility of free rotation and interactions of the apical carbonyl−benzyl−amine (or the corresponding carbonyl−benzylamine−dansyl group)

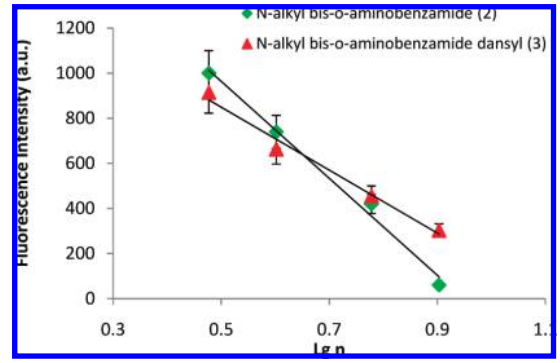

Figure 3. Fluorescence intensities at wavelength of maxima emission related to the number of carbons on the spacer group of *N*-alkyl-bis-*o*-aminobenzamide (**2**) and *N*-alkyl-bis-*o*-aminobenzamide dansyl (**3**) bound to Merrifield resin.

with the surroundings also increased, thus allowing nonradiative deactivation of the fluorophore.

Metal Ion Recognition Properties of *N*-Alkyl-bis-*o*-aminobenzamide and *N*-Alkyl-*o*-aminobenzamide Dansyl Materials. In order to evaluate the analytical potential of the **3**(**a**−**d**) bead series as sensing materials, two groups of metal ions were used as models: (a) alkali and alkaline earth cations (Li^+, Na^+, K^+, Ca^{2+}, and Mg^{2+}) and (b) transition metal ions (Fe^{3+}, Zn^{2+}, and Cu^{2+}). The beads were packed into a conventional flow-through fluorescence cell using a continuous flow-injection setup (Figure 4).

For the alkali and alkaline-earth metal ions, two interesting facts could be observed. First, cation binding was signaled by an increase in luminescence, particularly when the **3d** member of the series was used. Second, a preferential sensing of Mg^{2+} over the other cations by all the **3**(**a**−**d**) materials was evident (see Figure 5). Similar results were observed at pH 6−8. Further experiments were carried out at pH 7.7.

This behavior is consistent with the occurrence of a PET mechanism involving the nitrogen atoms (see Scheme 3). In the free complexing hosts (**2**-series), PET can occur between the lone pair of the amine group adjacent to the benzene ring and the excited dansyl moiety, thus giving rise to relatively low fluorescence intensity. The Weller equation[8] is a useful tool for predicting whether electron transfer will occur between the excited-state molecule and the ground-state molecule (eq 1):

$$\Delta G_{PET} = 23.06[(E_{ox} - E_{red}) - E_{oo} - e^2/\varepsilon r] \qquad (1)$$

where E_{ox} is the oxidation potential of a donor (e.g., electron rich group, amine lone pair), E_{red} is the reduction potential of the acceptor (e.g., an aryl group), E_{oo} is the singlet excited-state energy in electronvolts and $e^2/\varepsilon r$ is the attractive energy term related to the formation of a radical ion pair. This equation relates the driving force for the photoinduced electron transfer step (ΔG_{PET}) to the oxidation potential of the electron donor (E in volts), the reduction potential of the acceptor, and the excited-state energy of the component that absorbs the light (E_{oo} in kilocalories per mole). Under the assumption that the amine groups on the benzene rings and dansyl moieties have independent redox potentials, the free energy changes of PET can be roughly assessed from the Rohm−Weller equation. The oxidation potential of the amine groups bound to the benzene subunits can be ap-

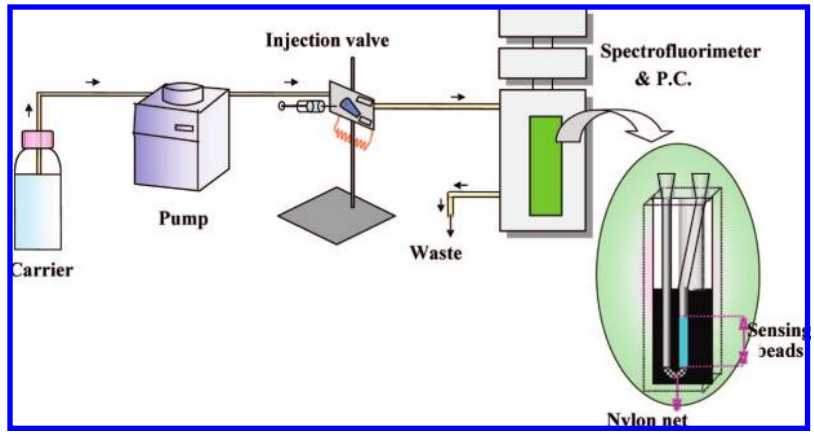

Figure 4. Flow-injection setup for screening the sensing beads.

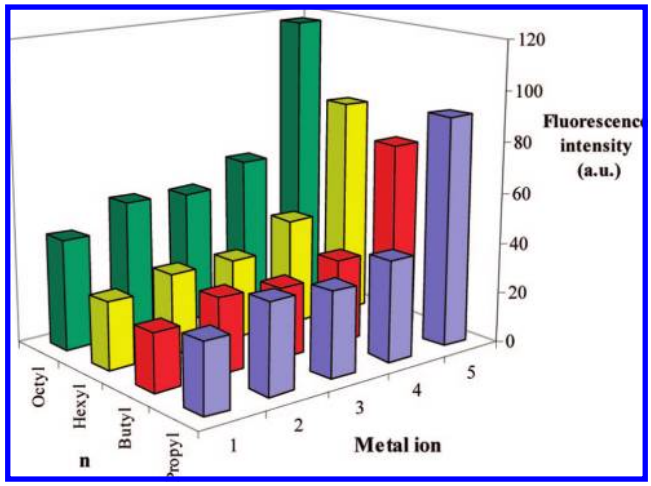

Figure 5. Fluorescence intensity of **3**(**a**−**d**) sensing materials upon metal ion complexation: (1) lithium, (2) sodium, (3) potassium, (4) calcium, (5) magnesium. A 125 μL portion of 1 M metal ion solution was injected.

proximated by the value for *N*-methylaniline[26] as 0.81 V vs standard calomel electrode (SCE) in acetonitrile. The reduction potential of the dansyl moiety can be approximated by the value for propyldansylamide[27] as −2.02 V vs SCE in acetonitrile. The singlet energy of the dansyl group was calculated as 2.8 eV from the average of the energies of the spectral maxima in absorption and emission. The attractive potential between the radical ion pair $e^2/\varepsilon r$ ranges between 0.1−0.2 eV.[28] An average value of 0.15 eV was used in this study. Application of these values into eq 1 yielded $\Delta G_{PET} = -2.80$ eV, which is a substantially negative value to guarantee the occurrence of the photoinduced electron transfer process on a thermodynamic basis. Upon addition of alkali and alkali-earth metal ions, an increase in the intensity of the dansyl fluorescence was observed due to the increased oxidation potential of the amine groups upon metal complexation.[29] Complexation therefore suppressed PET to the singlet, leading to an enhancement in dansyl fluorescence.

All attached compounds are flexible molecules that undergo conformational changes on complexation by wrapping around the metal ion. It is worth mentioning that the decrease in the intramolecular energy transfer was observed to scale with the charge of the alkaline and alkaline-earth ion: monocations gave ca. a 25−35-fold decrease in the energy transfer rate while dications yielded 300−5000-fold decrease,

Table 1. Ionic Radii and Surface Charge Density of Metal Cations[a]

metal ion	ionic radius (Å)	surface charge density ($Z = Å^{-2}$) ($Z = 1$ or 2)
Li^+	0.78	0.13
Na^+	0.98	0.085
K^+	1.33	0.045
Ca^{2+}	1.06	0.14
Mg^{2+}	0.78	0.26

[a] Data taken from ref 30.

for calcium and magnesium, respectively. Qualitatively, this trend may be attributed to the separation distance between the lumophor (dansyl group) and benzene groups being varied due to variations in Coulombic effects. In fact, according data in Table 1, the surface charge density as well as the charge/radius ratio of $Mg^{2+}$are higher than those for Ca^{2+} and much higher than for alkali-metal ions. Therefore, a higher rigidity of the pseudo cyclic structure of the complex may be expected due to a stronger interaction between donor groups and magnesium ions.

Concerning transition metal ions, complexation with Zn^{2+}, Fe^{3+}, and Cu^{2+} ions to **2** and **3** series leads to a quenching of the luminescence of the appended chromophors, most probably via a metal ion to benzene or dansyl PET mechanism, following the quenching effect $Cu^{2+} > Fe^{3+} > Zn^{2+}$. Taking into account the above results, the PET sensing ability of **2**- and **3**-series resins using a flow-through approach was then investigated for magnesium ions. The results obtained showed that the presence of the dansyl group (**3**-series) did not improve significantly the fluorescence response. The *o*-aminobenzamide unit provided by itself a high fluorescent group in the system for signaling the interaction with the corresponding metal ion. Notwithstanding, the presence of the dansyl group allowed to work at longer wavelengths, which was advantageous in order to avoid resin overlapping, thus enhancing the sensitivity of the sensing process.

Preliminary experiments were performed in order to evaluate the potential applicability of these materials. In Figure 6A, the flow response−time profile of the **3d** beads as signaling phase of Mg^{2+} metal ion standards is shown. The reversibility and reproducibility of the response are adequate enough to consider these simple systems as efficient fluorosensors for Mg^{2+}. In Figure 7B, the fluorescence calibration graphs for the **3c** and **3d** materials with increasing amounts of Mg^{2+} are shown. Detection limits for these

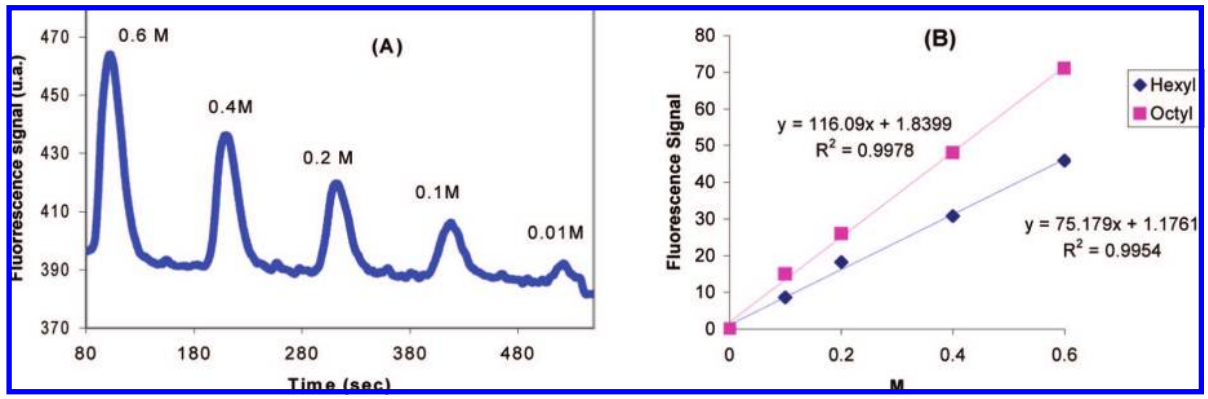

Figure 6. (A) Flow response−time profile of **3d** resin for different concentrations of Mg^{2+} standard solutions injected (injected volume =125 μL). (B) Calibration curves for Mg^{2+} standard solutions using **3c** and **3d** resins as sensing materials.

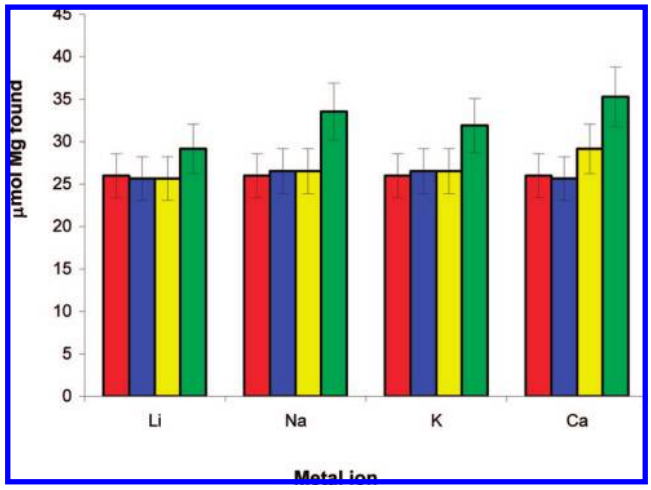

Figure 7. Effect of different metal ions on the magnesium determination at pH 7 (λ_{exc} = 432 nm λ_{em} = 375 nm): (red) Mg = 26 μmol; (blue) Mg = 26 μmol + metal ion = 12 μmol; (yellow) Mg = 26 μmol + metal ion = 26 μmol; (green) Mg = 26 μmol + metal ion = 52 μmol.

materials, calculated as the concentration corresponding to a signal that was three time the standard deviation of the blank signal, resulted to be 30 and 10 mM Mg^{2+}, respectively.

Study of Metal Ion Interference in the Determination of Mg(II). A metal ion interference study was conducted in a flow system (Figure 7) by injecting 26 μmoles of Mg^{2+} at pH 7 in presence of different concentrations of Li^+, Na^+, K^+, and Ca^{2+} (13, 26, and 52 μmoles) into the carrier flow stream.

As can be seen in Figure 7, for low ionic strength solutions, the octyl resin (**3d**) shows a preferential binding against Mg^{2+} over the other cations: recovery of magnesium ranges between 100 and 107% when the concentration of competing ions is below or similar to that of magnesium, while recoveries between 110 and 130% were observed when the concentration of the competing ions was twice that of magnesium. Determination of magnesium can be carried out in the presence of lower or similar amounts of Li^+, Na^+, K^+, and Ca^{2+} in a concentration range of 0.01−0.1 M.

Soil salinization is one of the major problems in agriculture, particularly in arid regions where drought, high temperatures, nutrient deficiency, and scarce precipitation go hand in hand. It remains a challenge to incorporate new sensing approaches for agriculture.[31] As other cations such as sodium, potassium, or calcium did not interfere in lower or similar concentrations the preliminary analytical evaluation of the systems described in this paper demonstrated that these materials could be useful for magnesium determination in salty samples, such as extracts of those salty soils. The rapid response of the system that allows samples to be analyzed within 60 s, and the low sample volumes required make the systems developed likely candidates for use in a real-time soil sensing system. Work in this direction is currently in progress.

In conclusion, bis-*o*-aminobenzamide dansyl resins were synthesized and their sensing properties for different metal cations were evaluated. The results demonstrated our main design principle that chemosensors based on the PET process can be developed on solid supports and that recognition can be fine-tuned by screening libraries that contain a variable recognition domain. There is no doubt that the development of these types of sensing systems on solid supports will produce novel prototype fluorescent chemosensor devices in the future.

Experimental Section

Materials. Merrifield resin (polystyrene backbone cross-linked with divinylbenzene) used in this work was purchased from Argonaut Technologies Inc. and have a load of 1.19 mmol/g. All other reagents, if not specified, were purchased from Aldrich. Chemicals, buffers, and solvents were of analytical reagent grade and were used without further purification. All aqueous solutions were prepared using deionized water. Standard working solutions of Na^+, K^+, Mg^{2+}, Cu^{2+}, Fe^{3+}, and Zn^{2+} at different concentrations were prepared in the buffer solution (pH 7).

Instrumentation. Melting points were obtained on an Electrothermal 88629 apparatus. Infrared (IR) spectra were recorded on a Perkin-Elmer FT-IR 1600 spectrometer. ^1H and ^{13}C nuclear magnetic resonance spectra were recorded on a Varian Mercury 200 spectrometer in $CDCl_3$ with TMS as internal standard, at 200 and 50.289 MHz, respectively. EI-Mass spectra were obtained on a Hewlett-Packard 5989 MS spectrometer at 70 eV by direct insertion. Combinatorial chemistry procedures were carried out in a Reactor Quest Argonaut model SLN-210. All fluorescence intensity measurements were made with a Shimadzu RF-5301 PC spectrometer provided with a xenon discharge excitation source.

The 3 nm slit width for both excitation and emission intensities were used. Instrumental parameters and processing data were controlled by the Fluorescence Data manager software. A single flow injection system equipped with a Hellma Model 176.52 flow cell (25 μL) was used for screening the sensing materials. Beads were washed free of any starting materials and solvent and packed into the flow-through cell. Measures of fluorescence intensities were obtained directly from the resin beads. All experiments were carried out at 20 ± 2 °C. pH measurements were made with an Orion Model 710A pH/ISE meter. Lead and copper were estimated by atomic absorption spectrometer using a Varian spectrometer AA-5 model with acetylene−air flame. Mass spectra were obtained on Agilent 1100 series LC/MSD.

Flow Injection Manifold and General Procedure. The experimental set up for the system is shown in Figure 4. A Minipuls 2 four-channel peristaltic pump (Gilson, Worthington, OH) was used to generate the flow stream. A type 50 PTFE four-way rotatory valve (Omnifit, Cambridge, UK) provided with a 125 μL sample loop was used for solution standard introduction. PTFE tubing (0.8 mm i.d.) and fittings were used for connecting the flow-through cell, the valve, and the carrier solution. The carrier buffers consisted of 0.1 mol L^{-1} tris (pH 7.7).

Calibration. Standard solutions of Mg^{2+} (consisting of carrier solution plus a known volume of the standard Mg^{2+}solution) were injected through the valve into the carrier flow stream. This stream was merged with the carrier mixed in the reaction coil and driven to the flow cell packed with immobilized resins. Typical fluorescence signals were obtained and were plotted against molar metal ion concentration.

General Method for the Synthesis of Alkyl-bis-*o*-aminobenzamide. Propyl-bis-*o*-aminobenzamide (1a). Isatoic anhydride (3 g, 18.4 mmol) was dissolved in 20 mL of DMF and cooled to 0 °C. Then, 1,3-propylendiamine (0.68 g, 9.2 mmol) was added dropwise under inert atmosphere conditions and the temperature was increased to 60 °C and stirred for 1 h. The reaction mixture was poured in hot water (100 mL), and the solid product was filtered and recrystallized in ethanol. A white solid was obtained (2.52 g, 88% yield). Mp. 171−172 °C. IR (KBr): 3471, 3362, 3300, 3062, 1627, 1582, 1300, 1264, 1150 cm^{-1}. ^{1}H NMR (DMSO-d_6, 200 MHz): δ 8.19 (t, J = 5.3 Hz, 2H, N*H*), 7.47 (dd, J = 7.9, 1.3 Hz, 2H, H-6), 7.13 (ddd, J = 8.3, 8.1, 0.9 Hz, 2H, H-4), 6.68 (dd, J = 8.3, 0.9 Hz, 2H, H-3), 6.51 (ddd, J = 8.3, 7.9, 0.9, 2H, H-5), 6.35 (brs, 4H, NH_2), 3.26 (td, J = 6.7, 5.5 Hz, 4H, CH_2-α), 1.74 (q, J = 6.8 Hz, 2H, CH_2-β). ^{13}C NMR (DMSO-d_6, 50 MHz,): δ 168.5 (C═O), 149.3 (C-2), 131.3 (C-4), 127.5 (C-6), 115.6 (C-5), 114.1 (C-1),113.4 (C-4), 36.7 (C-α), 29 (C-β). EIMS *m*/*z* (rel. int): 312 (M^+,100), 120 (50), 150 (34), 163 (25).

Butyl-bis-*o*-aminobenzamide (1b). (2.71 g, 90%). Mp. 199−200 °C. IR (KBr): 3480, 3374, 3296, 3056, 2938, 1625, 1584, 1320, 1266, 1156 cm^{-1}. ^{1}H NMR (DMSO-d_6, 200 MHz): δ 8.19 (t, J = 5.6, 2H, -N*H*), 7.46 (dd, J = 7.9, 1.3 Hz, 2H, H-6), 7.11 (ddd, J = 7.6, 7.1, 1.5 Hz, 2H, H-4), 6.67 (d, J = 7.5 Hz, 2H, H-3), 6.49 (dd, J = 7.9, 7.5 Hz, 2H, H-5), 6.37 (brs, 4H, NH_2), 3.23 (brd, J = 5.5 4H, CH_2-α), 1.54 (brs, 4H, CH_2-β). ^{13}C NMR (DMSO-d_6, 50 MHz): δ 168.6 (C═O), 149.3 (C-3), 131.3 (C-4), 127.9 (C-6), 116.1 (C-5), 114.9 (C-1), 114.4 (C-3), 38.5 (C-α), 26.8 (C-β). EIMS *m*/*z* (rel. int.): 326 (M^+, 100), 120 (70), 149 (34), 163 (25), 189 (50).

Hexyl-bis-*o*-aminobenzamide (1c). (2.77 g, 85%), Mp. 165 °C. IR (KBr): 3474, 3376, 3334, 3066, 2918, 1631, 1580, 1542, 1317, 1260, 1156 cm^{-1}. ^{1}H NMR (DMSO-d_6, 200 MHz): δ 8.16 (brt, J = 5.4 Hz, 2H, N*H*), 7.45 (d, J = 7.9 Hz, 2H, H-6), 7.11 (ddd, J = 8.3, 7.0, 1.2 Hz, 2H, H-4), 6.67 (d, J = 8.3 Hz, 2H, H-3), 6.49 (dd, J = 7.9, 7.1 Hz, 2H, H-5), 6.37 (brs, 4H, NH_2), 3.20 (td, J = 6.5, 6.1 Hz, 4H, CH_2-α), 1.51 (brt, 4H, CH_2-β), 1.33 (brs, 4H, CH_2-γ). ^{13}C NMR (DMSO-d_6, 50 MHz): δ 168.5 (C═O), 149.3 (C-2), 131.3 (C-4), 127.8 (C-6), 116.1 (C-5), 115.0 (C-1), 114.4 (C-3), 38.7 (C-α), 29.2 (C-β), 26.3 (C-γ). EIMS *m*/*z* (rel. int.): 354 (M^+, 28), 120 (100), 217 (20).

Octyl-bis-*o*-aminobenzamide (1d). (2.99 g, 85%), Mp. 175−177 °C. IR (KBr): 3475, 3364, 3296, 3067, 2927, 1625, 1580, 1544, 1318, 1262, 1155 cm^{-1}. ^{1}H NMR (DMSO-d_6, 200 MHz): δ 8.2 (t, J = 5.5 Hz, 2H, N*H*), 7.45 (dd, J = 7.9, 1.5 Hz, 2H, H-6), 7.12 (ddd, J = 8.2, 7.7, 1.5 Hz, 2H, H-4), 6.67 (dd, J = 8.2, 1.1 Hz, 2H, H-3), 6.50 (ddd, J = 7.9, 7.7, 1.1 Hz, 2H, H-5), 6.39 (brs, 4H, -NH_2), 3.19 (td, J = 6.5, 5.5, 4H, CH_2-α), 1.50 (m, 4H, CH_2-β), 1.30 (brs, 8H, H-CH_2-γ,δ). ^{13}C NMR (DMSO-d_6, 50 MHz): δ 168.5 (C═O), 149.3 (C═2), 131.3 (C—4H), 127.9 (C-6), 116.2 (C-1), 116.1 (C-5), 114.4 (C-3), 38.7 (C-α), 29.2 (C-β), 28.8 (C-δ), 26.5 (C-γ). EIMS *m*/*z* (rel. int.): 382 (M^+, 7), 120 (100).

General Method for the Synthesis of Alkyl-bis-*o*-aminobenzamide on Merrifield Resin. Propyl-bis-*o*-aminobenzamide Resin (2a). Merrifield resin (1.00 g, 1.19 mmol) was swelled for 30 min in 30 mL of DMF. Then, K_2CO_3 (4.11 g, 5.95 mmol) and a solution of propyl-bis-*o*-aminobenzamide (1.85 g, 5.95 mmol in 15 mL of DMF) were added at room temperature. The mixture was stirred for 6 h at 70 °C, and after cooling, it was filtered and washed with H_2O (3 × 25 mL), MeOH (3 × 25 mL), THF (3 × 25 mL), Et_2O (3 × 25 mL), and CH_2Cl_2 (3 × 25 mL). Finally, the resin was dried under vacuum. 960 mg (96% recuperation, 82% conversion). IR (KBr): 3453, 3353, 3021, 2918, 1654, 1600, 1492, 1451 cm^{-1}. FI = 1000 au, λ_{em} = 433 nm, λ_{exc} = 386 nm. EIMS *m*/*z* (rel. int.): 312 (M^+,100), 120 (50), 150 (34), 163 (25).

Butyl-bis-*o*-aminobenzamide Resin (2b). (95% recuperation, 80% conversion). IR (KBr): 3450, 3355, 3019, 2918, 1647, 11597, 1490, 1450 cm^{-1}. FI = 740 au, λ_{em} = 433 nm, λ_{exc} = 387 nm. EIMS *m*/*z* (rel. int.): 326 (M^+,100), 120 (70), 149 (34), 163 (25), 189 (50).

Hexyl-bis-*o*-aminobenzamide resin (2c). (96% recuperation, 84% conversion). IR (KBr): 3455, 3353, 3020, 2915, 1652, 1603, 1492, 1451 cm^{-1}. FI = 450 au, λ_{em} = 432 nm, λ_{exc} = 375 nm. EIMS *m*/*z* (rel. int.): 354 (M^+, 28), 120 (100), 217 (20).

Octyl-bis-*o*-aminobenzamide Resin (2d). (94% recuperation, 88% conversion). IR (KBr): 3449, 3348, 3025, 2915, 1652, 1605, 1490, 1455 cm^{-1}. FI = 60 au, λ_{em} = 432 nm, λ_{exc} = 375 nm. EIMS *m*/*z* (rel. int.): 382 (M^+, 7), 120 (100).

General Method for the Synthesis of Alkyl-bis-*o*-aminobenzamide Dansyl Resin. Propyl-bis-*o*-aminobenzamide Dansyl Resin (3a). Propyl-bis-*o*-aminobenzamide resin (960 mg, 0.94 mmol) was swelled for 30 min in 20 mL of dichloromethane. Then, 0.5 mL of triethylamine was added and the mixture was stirred at room temperature for 5 min. A solution of dansyl chloride (0.76 g, 2.82 mmol) in 5 mL dichloromethane was added and the mixture was refluxed for 1 h. The product was filtered to eliminate the excess of reagents and washed with MeOH (3 × 25 mL), Et_2O (3 × 25 mL), and CH_2Cl_2 (3 × 25 mL). Finally, the resin was dried under vacuum. Measures of fluorescence intensity were obtained directly from the resin beads. IR (KBr): 3336, 3024, 2916, 1654, 1605, 1490, 1455, 1304 cm^{-1}. FI = 914 au, λ_{em} = 497 nm, λ_{exc} = 389 nm.

Butyl-bis-*o*-aminobenzamide Dansyl Resin (3b). (94% recuperation, 88% conversion). IR (KBr): 3352, 3020, 2918, 1646, 1598, 1490, 1450, 1300 cm^{-1}. FI = 663 au, λ_{em} = 506 nm, λ_{exc} = 392 nm.

Hexyl-bis-*o*-aminobenzamide Dansyl Resin (3c). (94% recuperation, 88% conversion). IR (KBr): 3018, 2916, 1650, 1603, 1492, 1451, 1306 cm^{-1}. FI = 455 au, λ_{em} = 500 nm, λ_{exc} = 395 nm.

Octyl-bis-*o*-aminobenzamide Dansyl Resin (3d). (94% recuperation, 88% conversion). IR (KBr): 3340, 3020, 2918, 1656, 1605, 1490, 1455, 1300 cm^{-1}. FI = 303 au, λ_{em} = 515 nm, λ_{exc} = 410 nm.

Acknowledgment. We gratefully acknowledge the support for this project by Consejo Nacional de Ciencia y Tecnología, México (CONACyT, Grant No. SEP-CO1-47835-U) and Dirección General de Educación Superior Tecnologica (DGEST-2006). A.O.-T. thanks CONACyT for a graduate fellowship. Further, we thank Dra. Marta E. Diaz-Garcia for technical support.

References and Notes

(1) (a) Martínez-Manez, R.; Sancenon, F. *Chem. Rev.* **2003**, *103*, 4419–4476. (b) De Silva, A. P.; McClenaghan, N. D. *Chem.—Eur. J.* **2004**, *10*, 574–586.
(2) Boisdé, G.; Harmer, A. *Chemical and Biochemical Sensing with Optical Fibers and Waveguides*; Artech House, Inc: Norwood, MA, 1996.
(3) Hartley, J. H.; James, T. D.; Ward, C. J. *J. Chem. Soc., Perkin Trans.* **2000**, *1*, 3155–3184.
(4) Pina-Luis, G.; Granda Valdés, M.; Badía, R.; Díaz-García, M. E. *Analyst* **1998**, *123*, 155–158.
(5) Vélez, López, E.; Pina-Luis, G.; Suárez Rodríguez, J. L.; Rivero Espejel, I.; Díaz-García, M. E. *Sensors Actuators B* **2003**, *90*, 256–263.
(6) Rivero, I. A.; González, T.; Pina-Luis, G.; Díaz-García, M. E. *J. Comb. Chem.* **2005**, *6*, 46–53.
(7) Crespo-Otero, R.; Suardiaz, R.; Pina-Luis, G.; Granda Valdés, M.; Díaz-García, M. E.; Montero, L. A. *J. Mol. Struct. (Theochem)* **2008**, *852* (1−3), 71–77.
(8) Weller, A. *Pure Appl. Chem.* **1968**, *16*, 115–118.
(9) Mataga, N. *Pure Appl. Chem.* **1993**, *65*, 1605–1610.
(10) Valeur, B.; Leray, I. *Coord. Chem. Rev.* **2000**, *205*, 3–40.
(11) Carraway, E. R.; Demas, J. N.; De Graff, B. A. *Anal. Chem.* **1991**, *63*, 332.
(12) Velasco García, N.; Pereiro García, R.; Díaz-García, M. E. *Spectrochim. Acta* **1995**, *51A*, 895–904.
(13) Ayadim, M.; Jiwan, J. H. L.; Prassanna de Silva, A.; Soumillion, J.Ph. *Tetrahedron Lett.* **1996**, *37*, 7039–7042.
(14) Zhujun, Z.; Seitz, W. R. *Anal. Chim. Acta* **1985**, *171*, 251–8.
(15) Saari, L. A.; Seitz, W. R. *Anal. Chem.* **1983**, *55*, 667–670.
(16) Singh, A.; Yao, Q.; Tong, L.; Still, W. C.; Sames, D. *Tetrahedron Lett.* **2000**, *41*, 9601.
(17) Liu, Y.; Zong, L.; Zheng, L.; Wu, L.; Cheng, Y. *Polymer* **2007**, *48* (23), 6799–6807.
(18) Rivero, I. A.; González, T.; Pina-Luis, G.; Díaz-García, M. E. *Comb. Chem. High Throughput Screening* **2006**, *9*, 535–544.
(19) Pereiro García, M. R.; Díaz García, M. E.; Sanz-Medel, A. *Analyst,* **1990**, *115*, 575–579.
(20) Castillo, M.; Pina Luis, G.; Díaz-García, M. E.; Rivero Espejel, I. A. *J. Braz. Chem. Soc.* **2005**, *16* (3A), 412–417.
(21) Obrecht, D.; Villalgordo, J. M. *Solid-Supported Combinatorial and Parallel Synthesis of Small Molecular-Weight Compound Libraries*; Tetrahedron Organic Series; Pergamon Press: Oxford, 1998; Vol. 17.
(22) Dolle, R. E. *J. Comb. Chem.* **2000**, *2*, 383–433.
(23) Sammelson, R. E.; Kurth, M. J. *Chem. Rev.* **2001**, *101*, 137–202.
(24) (a) Harris, D. C. *Quantitative Chemical Analysis*, 5th ed.; Freeman W. H. and Company: New York, 1999. (b) Pina-Luis, G.; Badía, R.; Díaz-García, M. E.; Rivero, I. A. *J. Comb. Chem.* **2004**, *6*, 391–397.
(25) Chávez, D.; Ochoa, A.; Madrigal, D.; Castillo, M.; Espinoza, K.; González, T.; Vélez, E.; Meléndez, J. D.; Rivero, I. A. *J. Comb. Chem.* **2003**, *5*, 149–154.
(26) Porcal, G.; Bertolotti, S. G.; Previtali, C. M.; Encinas, M. V. *Phys. Chem. Chem. Phys.* **2003**, *5*, 4123–4128.
(27) Ceroni, P.; Laghi, I.; Maestri, M.; Balzani, V.; Gestermann, S.; Gorka, M.; Vögtle, F. *New J. Chem.* **2002**, *26*, 66–75.
(28) Grabowski, Z. R.; Dobkowski, J. *Pure Appl. Chem.* **1983**, *55*, 245–252.
(29) Prasanna de Silva, A.; Fox, D. B.; Moody, T. S.; Weir, S. M. *Pure Appl. Chem.* **2001**, *73*, 503–511.
(30) Lehn, J. M. Design of Organic Complexing Agents. Strategies towards Properties. *Structure and Bonding*; Springer-Verlag: Berlin, 1973; Vol. 16, Chapter 1.
(31) Barnes, E. M.; Sudduth, K. A.; Hummel, J. W.; Lesch, S. M.; Corwin, D. L.; Yang, C.; Daughtry, C. S. T.; Bausch, W. C. *Photogrammet. Eng. Remote Sensing* **2003**, *69*, 619–630.

CC8000772